
Article:
Li, M., Li, L., Zang, J. et al. (1 more author) (2015) Donor-doping and reduced leakage current in Nb-doped Na0.5Bi0.5TiO3. Applied Physics Letters, 106 (10). 102904. ISSN 0003-6951

https://doi.org/10.1063/1.4914509

Donor-doping and reduced leakage current in Nb-doped perovskite oxide $Na_{0.5}Bi_{0.5}TiO_3$

Ming Li[1], Linhao Li[1], Jiadong Zang[2], Derek C. Sinclair[1]*

[1]Department of Materials Science and Engineering, University of Sheffield, Sir Robert Hadfield Building, Mappin Street, Sheffield, S1 3JD, United Kingdom

[2]Institute of Materials Science, Technische Universität Darmstadt, Alarich-Weiss-Str. 2, 64287 Darmstadt, Germany

* Author to whom correspondence should be addressed.

E-mail: d.c.sinclair@sheffield.ac.uk

Abstract

Low levels of so-called 'donor-doping' in titanate-based perovskite oxides such as La for Ba,Sr and Nb for Ti in (Ba,Sr)TiO_3 can significantly reduce the resistivity of these typical (d^0) dielectric materials and expand application areas to positive temperature coefficient resistors, thermoelectrics, conductive wafers as thin film substrates and solid oxide fuel cell anode materials. Here we show low levels of Nb-doping (≤1 at%) on the Ti-site in the well-known lead-free piezoelectric perovskite oxide $Na_{0.5}Bi_{0.5}TiO_3$ (NBT) produces completely different behaviour whereby much higher resistivity is obtained, therefore indicating a different donor-doping (substitution) mechanism. There is a switch in conduction mechanism from oxygen-ions in undoped NBT with an activation energy (E_a) of < 0.9 eV to electronic (band gap) conduction in 0.5-1 at% Nb-doped NBT with E_a ~1.5-1.8 eV. This demonstrates the necessity of further systematic doping studies to elucidate the defect chemistry of NBT which is clearly different to that of (Ba,Sr)TiO_3. This defect chemistry needs to be understood if NBT-based materials are going to be manufactured on a large scale for commercial applications. This study also illustrates different donor-doping mechanisms to exist within the family of d^0 titanate-based perovskites.

Keywords: $Na_{0.5}Bi_{0.5}TiO_3$, $BaTiO_3$, piezoelectric, perovskite, impedance spectroscopy,

Titanate-based (d^0) perovskite oxides (Ba,Sr)TiO_3 are an important family of ferroelectric materials that have been widely used as ceramic capacitor materials for over 50 years.[1] Their technical importance has led to extensive studies on the effect of so-called 'donor' and 'acceptor' doping on the electrical properties and the associated defect chemistry in these titanates.[2] This has resulted in improved dielectric performance via optimised manufacturing processes with lower cost as well as discovery of new electrical phenomena and new application areas. For example, acceptor doping (replacing a host ion with a dopant of lower valence) in $BaTiO_3$ can improve the resistance to reduction when fired at low oxygen partial pressure (pO_2),[3, 4] thus making it possible to use base-metal electrodes (such as Ni, Cu) as compared to noble metals (such as Pt, Pd). This led to a revolution in the manufacturing of multilayer ceramic capacitor (MLCC) in the 1980s.[5] On the other hand, low levels (typically < 1 at%) of donor-doping (replacing a host ion with a dopant of higher valence) such as La at the Ba-site or Nb at the Ti-site in $BaTiO_3$ can dramatically transform this dielectric material into a n-type semiconductor with room temperature (RT) resistivity < 100 Ωcm.[6-8] This phenomenon has been explored to develop positive temperature coefficient resistors (PTCR).[8] For $SrTiO_3$, much lower resistivity (< 0.01 Ωcm at RT) can be achieved by donor-doping.[9] Nowadays highly conductive Nb-doped $SrTiO_3$ wafers are widely used as thin film substrates. The extremely high conductivity also makes donor-doped $SrTiO_3$ a promising candidate as an oxide-based thermoelectric material.[10] More recently, A-site deficient La-doped $SrTiO_3$ has been developed as a solid oxide fuel cell anode material.[11] Although debates on the origin(s) of the high conductivity remain,[12-14] it is clear that electrons are the dominating charge carrier.

We recently reported the d^0 perovskite titanate $Na_{0.5}Bi_{0.5}TiO_3$ (NBT) to behave very differently from (Ba,Sr)TiO_3.[15] Two types of electrically distinctive NBT compositions exist. Stoichiometric NBT exhibits intrinsic (band gap) electronic conduction with an activation

energy for conduction (E_a) ~1.7 eV. The stoichiometric NBT composition can be obtained by adding small amount of excess Bi (2 at%) in the starting composition to compensate for Bi-loss during sample processing. If the starting composition is stoichiometric or slightly Bi-deficient (2 at%), the final composition in the processed ceramics is Bi-deficient. The Bi deficiency in the final composition is low, as suggested by the presence of a secondary phase for a starting composition with 2 at% Bi deficiency. Nevertheless, such small compositional variations dramatically switch the electronic conduction in stoichiometric NBT to oxide-ion conduction in Bi-deficient NBT, accompanied with a decrease of E_a for the grain (bulk) conduction to <0.9 eV and with a significant increase in conductivity by more than three orders of magnitude below 600 °C. This behaviour was unexpected and demonstrated NBT to have very different defect chemistry compared to (Ba,Sr)TiO_3.

Over the past decade, there has been sharp increase in studies on NBT and related materials.[16-27] Most of the reports in the literature focus on optimisation of dielectric and piezoelectric properties by developing solid solutions with other ferroelectric materials. There are few reports on the dielectric and piezoelectric properties in donor (Nb, Ta)-doped NBT.[28-31] Here we report the effect on the electrical properties of Nb donor-doping on the Ti-site in NBT ceramics.

Compositions based on the general formula $Na_{0.5}Bi_{0.5}Ti_{1-x}Nb_xO_3$ (x=0.005, 0.01, 0.02, 0.03) were prepared using the solid state reaction method. Raw materials were predried before weighing and appropriate mixtures of powders were ball milled. Calcination was carried out at 800 ^oC with a further heat treatment 850 °C, both for 2 h each. Pellets were sintered at 1150 °C for 2 h. More details can be found in a previous report.[15] Phase purity was examined by X-ray diffraction (XRD) using a high-resolution STOE STADI-P diffractometer equipped with a linear position sensitive detector and operated with Cu $K_{\alpha 1}$ radiation.

Ceramic microstructure and compositional analyses were performed using a scanning electron microscope (SEM) JEOL 6400 equipped with an Oxford Link ISIS energy dispersive x-ray spectroscopy (EDS) detector. High temperature Impedance Spectroscopy (IS) measurements were performed in a non-inductively wound tube furnace using an Agilent E4980A, an HP 4192A impedance analyser and a Solartron 1260 system. Au paste (fired at 800 ^{o}C for 2 h) electrodes were used and IS data were corrected for sample geometry (thickness/area of pellet) and analysed using ZView software. Polarisation-Electric field (P-E) measurements were performed using an aixACCT TF Analyzer 2000 E system.

Similar to that observed in a previous report,[28] the Nb-doping limit in $Na_{0.5}Bi_{0.5}Ti_{1-x}Nb_xO_3$ is low. XRD and SEM/EDS data (not shown) reveal the presence of small amount of $Bi_2Ti_2O_7$-related secondary phase for $x \geq 0.02$. However, even 1 at% Nb-doping significantly increase the bulk resistivity (R_b) at 600 °C from ~ 800 Ω cm for undoped NBT to ~ 620 kΩ cm, as shown by the diameter of the high frequency arc in the impedance complex plane (Z*) plots, Fig.1a. A typical Z* plot for x = 0.01 at 600 °C consists of a single arc with an associated capacitance (C) of ~ 88 pF cm^{-1}, corresponding to ε_r ~994. The high ε_r value is consistent with the ferroelectric behaviour of NBT, confirming the arc is associated with the grain (bulk) response. The Z* plot of undoped NBT at 600 °C in air (see Fig. 2a-b in Ref.[15]) consists of bulk, grain boundary and electrode responses. With 1 at% Nb doping, the ceramic becomes electrically homogeneous, as shown by the frequency coincidence for the Z" and M" Debye peak maximum in the combined spectroscopic plot, Fig. 1b.

The Z* plot at 700 °C under different atmospheres for the Nb-doped ceramic shows R_b decreases with measuring pO_2 from ~56 kΩ cm in flowing O_2 to ~ 3 kΩ cm in N_2, Fig 1c. IS measurements were performed down to 0.01 Hz and there was no clear evidence for the presence of a spike and/or arc associated with Warburg diffusion and oxide ion conduction in

the Nb-doped ceramic. The pO_2 dependence of R_b and absence of any low frequency Warburg response suggests the dominance of n-type electronic conduction in the Nb-doped sample.

The temperature dependence of R_b for all samples are summarised in an Arrhenius plot of the bulk conductivity (σ_b) where $\sigma_b = 1/R_b$, Fig. 2. Clearly, R_b is very sensitive to Nb-doping and increases by more than three orders of magnitude at temperatures ≤ 500 °C and E_a increases to ~1.5 eV with only 0.5 at% Nb doping. E_a increases to ~ 1.8 eV at higher doping levels. An E_a of 1.5-1.8 eV is about half the optical band gap of ~ 3.0-3.5 eV reported in the literature,[32-34] suggesting the electronic conduction is close to intrinsic (band gap) behaviour.

The relative permittivity maximum ($\varepsilon_{r,max}$) decreases from ~ 3000 for undoped NBT to ~ 2800 for x = 0.005 and 0.01. Further increasing of x to 0.02 and 0.03 decreases $\varepsilon_{r,max}$ to ~2400; however the temperature of $\varepsilon_{r,max}$ (T_{max}) is similar for all samples. A significant change is observed for the dielectric loss (tan δ) where it increases sharply above ~ 300 ^oC for undoped NBT due to the high level of oxide-ion conductivity, Fig 3b. In contrast, Nb-doped samples exhibit tan δ < 0.005 at 300 - 600 °C, Fig. 3b-c. The loss peak maximum shifts to lower temperature from ~ 220 °C for undoped NBT to ~ 125-130° for x = 0.005 and 0.01 and to 80-90 °C for x = 0.02 and 0.03, Fig. 3b.

Careful examination of loss data at ~ 500 °C reveals there is another loss peak in x = 0.01 – 0.03. A highest loss peak maximum of ~0.005 is observed for x = 0.03. In less resistive samples, such a loss peak, if present, is masked by the high loss associated with high leakage current and is therefore not observable. The origin of this loss peak is presumably associated with the tetragonal-cubic phase transition in NBT that has been reported to occur at ~ 500-540 °C.[35, 36]

Hysteresis loops from P-E measurements show Nb-doping to influence the remanent polarization (P_r) and coercive field (E_c). P_r initially increases from 38.8 μC/cm^2 for undoped NBT to 40.2 μC/cm^2 for x = 0.005 and to 42.8 μC/cm^2 for x = 0.01, then it decreases to 37.8 μC/cm^2 for x = 0.02 and 34.5 μC/cm^2 for x = 0.03. E_c decreases with increasing x, from ~ 53 kV/cm for undoped NBT to ~ 37 kV/cm for x = 0.03.

The IS results reveal NBT ceramics become significantly more resistive and electrically homogeneous by low levels of Nb-doping, Figs. 1 and 2. This behaviour is strikingly different from that commonly observed in (Ba,Sr)TiO_3-related titanates,[2, 6, 7] where low levels of donor-doping induces substantial levels of semiconductivity. In a previous study,[15] we confirmed the high leakage current in NBT is associated with oxide ion conduction rather than electronic conduction. Bismuth and oxygen vacancies are generated through a loss of a small amount of Bi_2O_3 during ceramic processing, as given in the following Kroger-Vink equation:

$$2Bi_{Bi}^{\times} + 3O_O^{\times} \rightarrow 2V_{Bi}^{'''} + 3V_O^{\bullet\bullet} + Bi_2O_3 \qquad (1)$$

Donor-doping (such as Nb^{5+} at Ti-site) can fill up the oxygen vacancies according to equation:

$$Nb_2O_5 + V_O^{\bullet\bullet} \rightarrow 2Nb_{Ti}^{\bullet} + 5O_O^{\times} \qquad (2)$$

The overall reaction is:

$$2Bi_{Bi}^{\times} + 3O_O^{\times} + 3Nb_2O_5 \rightarrow 2V_{Bi}^{'''} + 6Nb_{Ti}^{\bullet} + 15O_O^{\times} + Bi_2O_3 \qquad (3)$$

Thus the oxide ion conductivity is suppressed and Nb-doped ceramics exhibit near intrinsic electronic conduction. It is interesting to note that the presence of oxygen (and also bismuth) vacancies in NBT is effective in switching the Nb donor-doping substitution mechanism from electronic as observed in (Ba,Sr)TiO_3 to ionic compensation. A further contributing factor is

the difference in their band structures. The $6s^2$ electron lone pairs associated with the Bi-ions are involved in hybridisation with the 2p orbitals associated with the O-ions and therefore the valence band in NBT has significant cation character. In $(Ba,Sr)TiO_3$ there are no electron lone pairs associated with the A-site cations and the valence band is based only on anion character. As shown by Klein et al,[37] this influences the relative energy levels of the valence and conduction bands and may inhibit the formation of Nb electronic donor-states and therefore high level of n-type electronic conductivity in NBT.

The Bi_2O_3 loss in NBT during sample processing is 'accidental' and therefore difficult to control in a reproducible manner. The loss is also very small and is challenging to quantify. Equation (3) can be used to estimate the bismuth and oxygen vacancy concentration. Our results show NBT (under the processing conditions employed in our studies) becomes highly resistive for x = 0.005-0.01 in $Na_{0.5}Bi_{0.5}Ti_{1-x}Nb_xO_3$. Based on equation (3), the bismuth and oxygen nonstoichiometry in NBT is in the range of 0.0017-0.0033 for bismuth and 0.0025-0.0050 for oxygen, corresponding to a formula of $Na_{0.5}Bi_{0.4967-0.4983}TiO_{2.995-2.9975}$. This demonstrates again the highly sensitive relationship between nonstoichiometry and electrical properties in NBT.

The extensive studies on NBT and related materials over the past decade have optimised solid solutions between NBT, $BaTiO_3$ and KNN for piezoelectric and high temperature capacitor applications.[19-25] The development history of $(Ba,Sr)TiO_3$-type devices[1-8] is based on the crucial importance of understanding the defect chemistry to optimise and accurately control the composition(s) with various donor and acceptor dopants for better performance and low cost and for reproducible, large scale manufacturing. This work and our previous study[15] show NBT has a different defect chemistry to $(Ba,Sr)TiO_3$ and is presumably linked to small but significant variations in A-site non-stoichiometry in NBT

that doesn't exist to any appreciable extent in (Ba,Sr)TiO_3-based systems. The knowledge of defect chemistry accumulated for (Ba,Sr)TiO_3 can't therefore be directly applied to NBT-related materials. Clearly more systematic work on the defect chemistry of donor and acceptor doping in NBT-based solid solutions is needed prior to any large scale industrial manufacturing of NBT-based devices in the near future.

Acknowledgements We thank the EPSRC for funding EP/L027348/1.

References

1. A. J. Moulson and J. M. Herbert, Electroceramics: materials, properties, applications, 2 ed. (John Wiley and Sons Ltd, 2003).

2. D. M. Smyth, The defect chemistry of metal oxides. (Oxford University Press, New York, 2000).

3. I. Burn and G. H. Maher, J. Mater. Sci. **10**, 633 (1975).

4. Y. H. Han, J. B. Appleby and D. M. Smyth, J. Am. Ceram. Soc. **70**, 96 (1987).

5. H. Kishi, Y. Mizuno and H. Chazono, Jpn. J. Appl. Phys. **42**, 1 (2003).

6. O. Saburi, J. Phys. Soc. Jpn. **14**, 1159 (1959).

7. G. H. Jonker, Solid State Electron. **7**, 895 (1964).

8. B. Huybrechts, K. Ishizaki and M. Takata, J. Mater. Sci. **30**, 2463 (1995).

9. T. Tomio, H. Miki, H. Tabata, T. Kawai and S. Kawai, J. Appl. Phys. **76**, 5886 (1994).

10. S. Ohta, T. Nomura, H. Ohta and K. Koumoto, J. Appl. Phys. **97** (2005).

11. D. Neagu and J. T. S. Irvine, Chem. Mater. **22**, 5042 (2010).

12. F. D. Morrison, D. C. Sinclair and A. R. West, J. Appl. Phys. **86**, 6355 (1999).

13. C. L. Freeman, J. A. Dawson, H. R. Chen, J. H. Harding, L. B. Ben and D. C. Sinclair, J. Mater. Chem. **21**, 4861 (2011).

14. I. Akin, M. Li, Z. Lu and D. C. Sinclair, RSC Adv. **4**, 32549 (2014).

15. M. Li, M. J. Pietrowski, R. A. De Souza, H. Zhang, I. M. Reaney, S. N. Cook, J. A. Kilner and D. C. Sinclair, Nat. Mater. **13**, 31 (2014).

16. T. R. Shrout and S. J. Zhang, J. Electroceram. **19**, 111 (2007).

17. T. Takenaka, H. Nagata and Y. Hiruma, Jpn. J. Appl. Phys. **47**, 3787 (2008).

18. J. Rödel, W. Jo, K. T. P. Seifert, E. M. Anton, T. Granzow and D. Damjanovic, J. Am. Ceram. Soc. **92**, 1153 (2009).

19. X. X. Wang, X. G. Tang and H. L. W. Chan, Appl. Phys. Lett. **85**, 91 (2004).

20. S. T. Zhang, A. B. Kounga, E. Aulbach, T. Granzow, W. Jo, H. J. Kleebe and J. Rödel, J. Appl. Phys. **103**, 034107 (2008).

21. Y. Hiruma, H. Nagata and T. Takenaka, J. Appl. Phys. **105**, 084112 (2009).

22. E. A. Patterson, D. P. Cann, J. Pokorny and I. M. Reaney, J. Appl. Phys. **111**, 094105 (2012).

23. R. Dittmer, E.-M. Anton, W. Jo, H. Simons, J. E. Daniels, M. Hoffman, J. Pokorny, I. M. Reaney and J. Rödel, J. Am. Ceram. Soc. **95**, 3519 (2012).

24. J. Zang, W. Jo, H. Zhang and J. Rödel, J. Eur. Ceram. Soc. **34**, 43 (2014).

25. E. Sapper, R. Dittmer, D. Damjanovic, E. Erdem, D. J. Keeble, W. Jo, T. Granzow and J. Rödel, J. Appl. Phys. **116**, 12 (2014).

26. J. Carter, E. Aksel, T. Iamsasri, J. S. Forrester, J. Chen and J. L. Jones, Appl. Phys. Lett. **104** (2014).

27. W. W. Ge, C. T. Luo, Q. H. Zhang, Y. Ren, J. F. Li, H. S. Luo and D. Viehland, Appl. Phys. Lett. **105**, 5 (2014).

28. H. G. Yeo, Y. S. Sung, T. K. Song, J. H. Cho, M. H. Kim and T. G. Park, J Korean Phys Soc. **54**, 896 (2009).

29. R. Zuo, H. Wang, B. Ma and L. Li, J. Mater. Sci. - Mater. Electron. **20**, 1140 (2009).

30. K. Kumar and B. Kumar, Ceram. Int. **38**, 1157 (2012).

31. N. Petnoi, P. Bomlai, S. Jiansirisomboon and A. Watcharapasorn, Ceram. Int. **39**, S113 (2013).

32. M. Bousquet, J. R. Duclere, E. Orhan, A. Boulle, C. Bachelet and C. Champeaux, J. Appl. Phys. **107**, 104107 (2010).

33. C. Y. Kim, T. Sekino and K. Niihara, J. Sol-Gel Sci. Technol. **55**, 306 (2010).

34. M. Zeng, S. W. Or and H. L. W. Chan, J. Appl. Phys. **107**, 043513 (2010).

35. G. O. Jones and P. A. Thomas, Acta Crystallogr., Sect. B: Struct. Sci **58**, 168 (2002).

36. G. Trolliard and V. Dorcet, Chem. Mater. **20**, 5074 (2008).

37. S. Y. Li, J. Morasch, A. Klein, C. Chirila, L. Pintilie, L. C. Jia, K. Ellmer, M. Naderer, K. Reichmann, M. Gröting and K. Albe, Phys. Rev. B **88**, 045428 (2013).

Figure captions:

FIG.1. (a) Z* plots and (b) combined Z" and M" spectroscopic plots of x = 0.01 at 600 °C. Inset in (a) shows the bulk response of undoped NBT (x = 0) on an expanded scale. (c) Z* plots for x = 0.01 at 700 °C under different atmospheres. Inset shows the data for measurements in N_2 on an expanded scale. Filled symbols indicate selected frequencies.

FIG.2. Arrhenius-type plots of bulk conductivity for all $Na_{0.5}Bi_{0.5}Ti_{1-x}Nb_xO_3$ samples.

FIG. 3. Temperature dependence of (a) ε_r and (b) tan δ at 1 MHz. (c) expanded view of tan δ at 300-600 °C for all $Na_{0.5}Bi_{0.5}Ti_{1-x}Nb_xO_3$ samples.

FIG. 4 Polarisation-electric field (P-E) hysteresis loops measured at 0.1 Hz and up to 100 kV/cm for all $Na_{0.5}Bi_{0.5}Ti_{1-x}Nb_xO_3$ samples.

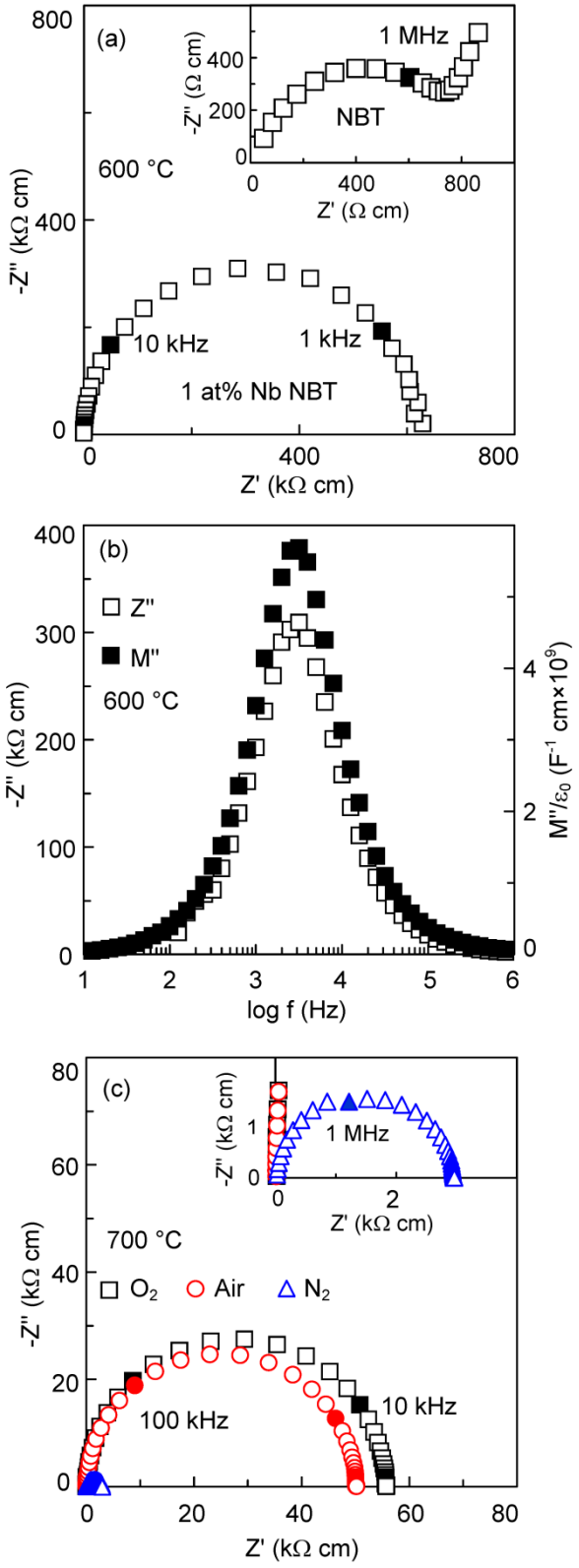
(a)
600 °C
1 MHz
NBT
-Z'' (Ω cm)
Z' (Ω cm)
10 kHz
1 kHz
1 at% Nb NBT
-Z'' (kΩ cm)
Z' (kΩ cm)
(b)
Z''
M''
600 °C
-Z'' (kΩ cm)
M''/ε0 (F-1 cm×10^9)
log f (Hz)
(c)
1 MHz
-Z'' (kΩ cm)
Z' (kΩ cm)
700 °C
O2
Air
N2
100 kHz
10 kHz
-Z'' (kΩ cm)
Z' (kΩ cm)

FIG.1

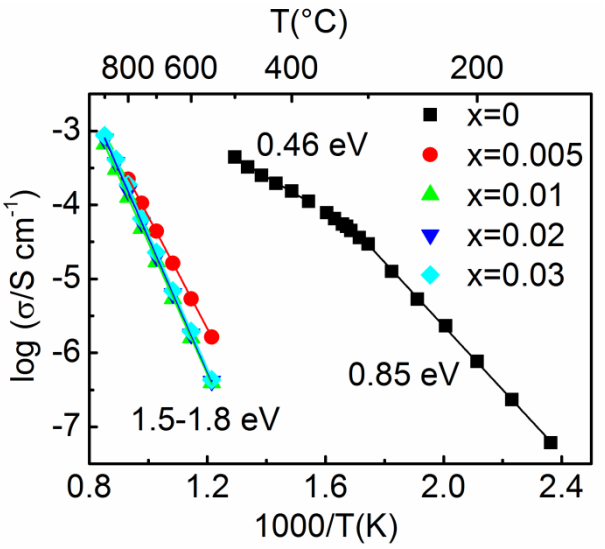
T(°C)
800 600
400
200
x=0
x=0.005
x=0.01
x=0.02
x=0.03
0.46 eV
0.85 eV
1.5-1.8 eV
log (σ/S cm-1)
-3
-4
-5
-6
-7
0.8
1.2
1.6
2.0
2.4
1000/T(K)

FIG.2

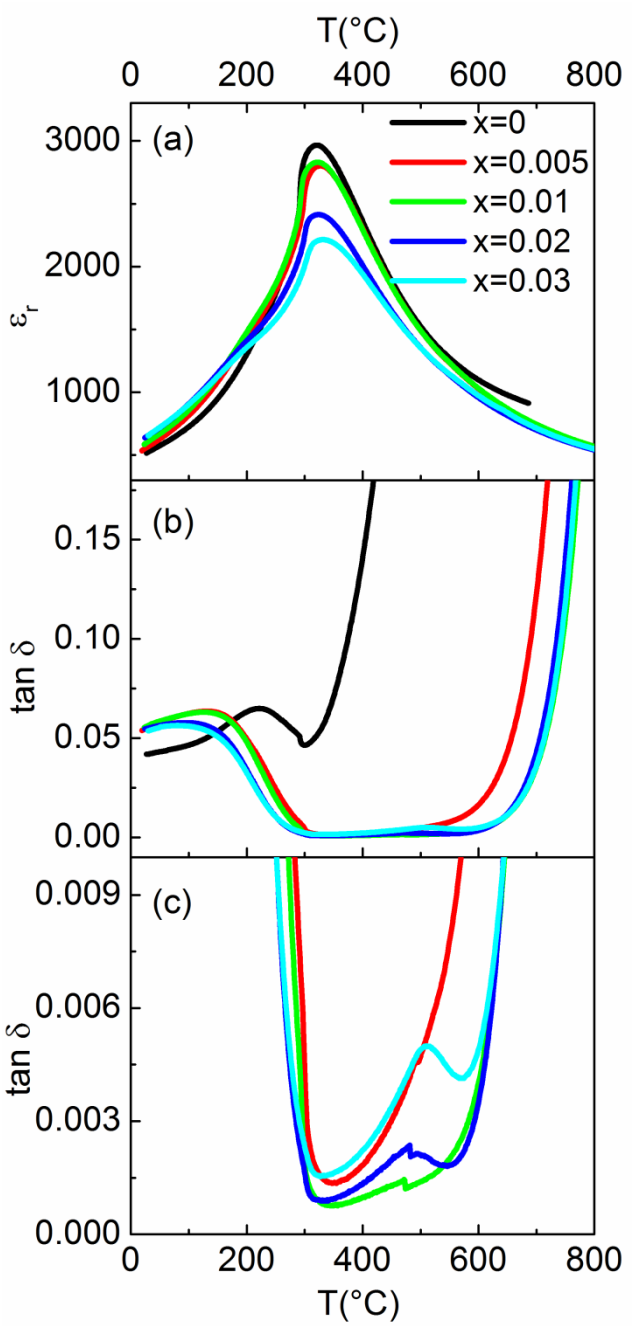
T(°C)
0
200
400
600
800
(a)
x=0
x=0.005
x=0.01
x=0.02
x=0.03
3000
2000
1000
ε_r
(b)
0.15
0.10
0.05
0.00
tan δ
(c)
0.009
0.006
0.003
0.000
tan δ
0
200
400
600
800
T(°C)

FIG. 3

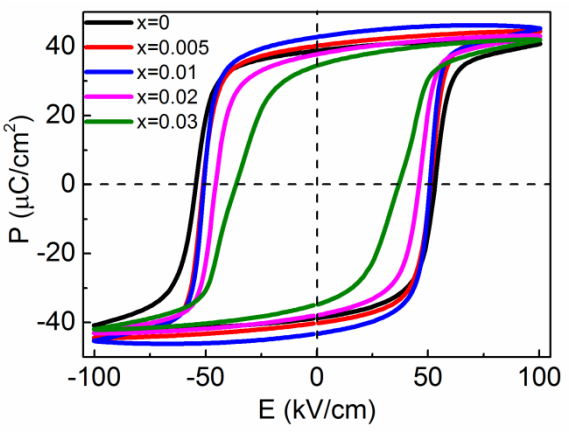
x=0
x=0.005
x=0.01
x=0.02
x=0.03
40
20
0
-20
-40
P (μC/cm²)
-100
-50
0
50
100
E (kV/cm)

FIG. 4